Prebifurcation noise amplification in a fiber laser

G. Huerta-Cuellar, A. N. Pisarchik, A. V. Kir'yanov, Yu. O. Barmenkov, and J. del Valle Hernández
Centro de Investigaciones en Optica, Loma del Bosque 115, Lomas del Campestre, 37150 Leon, Guanajuato, Mexico
(Received 15 September 2008; published 18 March 2009)

We report on the experimental evidence of noise amplification in an erbium-doped fiber laser in the vicinity of saddle-node, period-doubling, and crisis bifurcations. We demonstrate this interesting phenomenon by analyzing the laser bifurcation diagrams and power spectra. Numerical simulations on the base of an advanced laser model display good agreement with the experimental results.

DOI: 10.1103/PhysRevE.79.036204 PACS number(s): 05.45.−a, 42.55.Wd, 42.60.Mi

I. INTRODUCTION

The interaction between stochasticity and nonlinearity is a central current issue in the study of different dynamical systems including radiophysical [1], climatic [2,3], populational [4], geophysical [5], epidemical [6], and optical models [7]. Several experimental and theoretical works have demonstrated that this interaction sometimes plays a positive role in multistable systems, e.g., inducing stochastic [8], coherence [9] and vibrational [10] resonances, preference of attractors [11–14], attractor hopping [15,16], noise-enhanced multistability [17,18], etc. The idea that a system near the onset of a dynamical instability might be very sensitive to coherent or random perturbations originally came up in the Wiesenfeld and McNamara [19,20] papers. They showed that time-periodic dynamical systems can greatly amplify small-amplitude perturbations in the vicinity of the simplest classes of codimensional one bifurcations such as saddle-node, transcritical, pitchfork, period doubling, and Hopf. Later, small-signal amplification near the period-doubling bifurcation has been observed experimentally in a loss-modulated CO_2 laser [21].

Prebifurcation noise amplification has been extensively studied theoretically, using both linear [19] and nonlinear theories [22–25]. The linear theory displays an infinite growth of perturbations, as the system approaches the bifurcation point [19], whereas the nonlinear theories demonstrate a saturation effect near the period-doubling [22–24] and pitchfork [5,23] bifurcations; the real part of one of the negative Lyapunov exponents becomes positive when the system approaches the bifurcation point [22]. According to the Wiesenfeld's [19] theory, the prebifurcation noise amplification can serve as a noise precursor of the bifurcation in a nonlinear system; the addition of white noise gives rise to new broadband peaks not present in the noise-free system [19,26]. These noise precursor peaks are centered at new frequencies that appear only after the bifurcation. It is indeed of great practical importance to know how far the system is from a critical point. It is expected that strong changes in noise amplification anticipate many oncoming natural and biological catastrophes, such as tornado, earthquakes, convulsion of nature, epidemics, population extinction, myocardial infarction, etc., and thus can serve as an indicator of the adverse natural phenomena and diseases. For example, the sensitivity of the population to noise when close to a bifurcation has wide-ranging consequences for the evolution and ecology of population dynamics [4]. Some recent studies indicate an important role played by random atmospheric (such as westerly wind bursts) in sustaining the weakly damped southern oscillation, whose complementary warm and cold phases are, respectively, El Niño and La Niña [2]. The dynamics of childhood diseases have provided influential space studies to develop stochastic theoretical models with practical application to epidemiology. Childhood diseases are known to fall into regions of parameter space of high noise amplification [6]. Furthermore, multiple data on the main homeostatic constants, such as the glycemia level, body temperature, pH, etc., indicate that the fluctuation of these parameters during the day is an important diagnostic tool to predict how a disease will end. A severe sepsis with a septic shock is accompanied by an increase in the fluctuation range of the glucose level in spite of unavailing therapeutic efforts to maintain the homeostatic constant within its physiological region [27]. A systematic experimental study of the influence of noise on the dynamics of natural and biological systems is hard to realize because it is extremely difficult or even impossible to control their parameters.

Previous experiments in which noise amplification near bifurcation points was shown have not been directly devoted to the investigation of that certain phenomenon. For example, the noise rise effect near a bifurcation in experiments with a driven nonlinear electrical resonator was observed by Bocko and Battiato [28] in 1988 together with deamplification input random noise under certain conditions in the nonlinear system. Another experiment of Lamela *et al.* [29] with modulated diode lasers showed that noise can induce precursors of a virtual Hopf phenomenon near period-doubling bifurcations. However, the phenomenon of noise amplification in a nonlinear system close to the bifurcation points deserves to be a subject of separate consideration in experimental preparations.

Lasers have proved to be very useful tools for studying many nonlinear dynamical phenomena because their parameters can be easily controlled to determine the laser dynamics. It is well known that due to spontaneous emission of radiation and noisy parameters, e.g., the pump parameter, intrinsic noise is always present in any laser. In this work, we show how intrinsic and additional white noise applied to the diode pump current of an erbium-doped fiber laser (EDFL) behaves in the proximity of different bifurcations such as saddle-node, period doubling, and crisis points. In this paper, we provide an experimental evidence of prebifurcation noise amplification in a real physical system. We also develop an

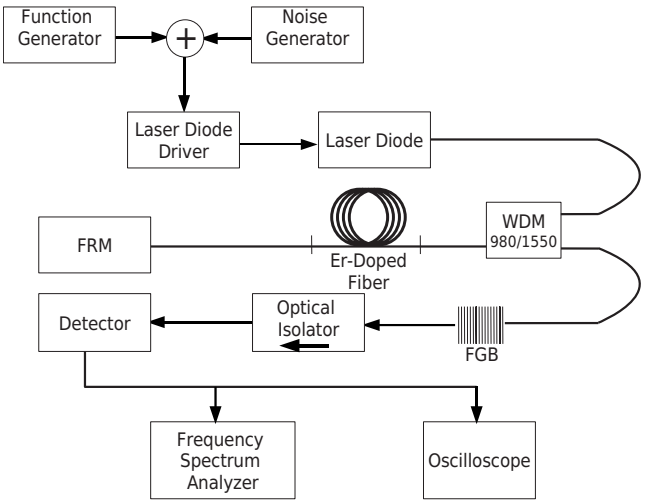

FIG. 1. Experimental setup. FRM stands for Faraday rotating mirror, FBG for fiber Bragg grating, and WDM for wavelength-division multiplexer.

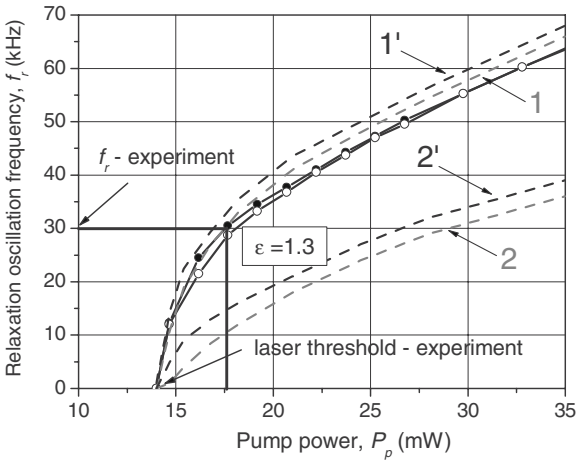

FIG. 2. Experimental (solid lines) and numerical (dashed lines) dependences of EDFL relaxation oscillation frequency on pump power. The experimental curves are obtained with intrinsic laser noise (open dots) and with 50%-modulation depth external noise (filled dots). The theoretical curves 1 and 1′ are calculated taking into account ASE and the curves 2 and 2′ without ASE. The curves 1 and 2 are obtained in the presence of noise and the curves 1′ and 2′ without it. The calculated f_r with ASE coincides with the experimentally measured one (at $\varepsilon=1.3$).

advanced EDFL model to better describe the laser behavior.

The paper is organized as follows. In Sec. II we describe the experimental setup and study experimentally the phenomenon of prebifurcation noise amplification in the vicinity of the saddle-node, period-doubling, and crisis points. The theoretical EDFL model and the results of numerical simulations are presented in Sec. III. We also demonstrate the validity of our model by comparing its results on some important laser characteristics, with those obtained experimentally. Finally, the main conclusions are given in Sec. IV.

II. EXPERIMENT

Due to excellent optical properties of erbium-doped fibers (high gain and single-mode operation), EDFL is widely used as a light source for optical communications, reflectometry, sensing, medicine, etc. [30] On the other hand, EDFL is a complex dynamical system, which serves as a paradigm for studying many nonlinear dynamical phenomena such as bifurcations, chaos, frequency locking, and multistability [31–37].

A. Experimental setup

In this paper, we use a 1560-nm EDFL subject to harmonic modulation of a 977-nm diode pump laser (Fig. 1). A 3.51-m Fabry-Perot laser cavity is formed by an active heavily doped 82-cm-long erbium fiber, a Faraday rotating mirror (FRM), and a fiber Bragg grating (FBG) with a 100-pm full width at half maximum (FWHM) bandwidth, having, respectively, 100% and 91% reflectivities for the laser wavelength. FRM is used to prevent the polarization mode beating, which can result in additional complexity of the laser system. The fiber laser output after passing through a wavelength-division multiplexer (WDM) is recorded with a photodetector and analyzed with an oscilloscope and a Fourier spectrum analyzer. In our experiments, the diode current is fixed at $I=69$ mA that results in the pump power $P=18$ mW which corresponds to about a 30% excess over the laser threshold $P_{\mathrm{th}}=14$ mW. The harmonic signal $A\sin(2\pi f_m t)$ (A and f_m being the amplitude and frequency of external modulation, respectively) is obtained from a signal generator, whereas the additive white noise $n\zeta$ (n and ζ being the external noise amplitude and a randomly generated number, respectively) comes from a noise generator; both are applied simultaneously to the diode pump driver current.

Without external modulation ($A=0$), EDFL exhibits small-amplitude oscillations (1%–2% of the magnitude of the steady-state power) at the relaxation oscillation frequency f_r which depends on the pump power and noise as shown in Fig. 2; the appearance of this frequency in the spectrum is due to the diode pump-laser intrinsic noise [38]. One can see that the additive noise slightly increases f_r. In our experiments, we choose the pump current so that the laser relaxation oscillation frequency f_r is about 30 kHz in the absence of the external noise. In the same figure, we plot also the numerically calculated dependence discussed in more details in Sec. III B.

B. Experimental results

Figure 3 shows the experimental bifurcation diagram of the peak-to-peak laser intensity with the modulation frequency f_m as a control parameter, for $A=8$ dB (units of the noise generator) that corresponds to a 25% modulation depth of the pump current in the absence of external noise ($n=0$). One can see the coexistence of different periodic and chaotic attractors for certain modulation frequencies. We construct this diagram changing the initial conditions either by switching on and off the signal generator or by increasing and decreasing f_m. As mentioned in some previous papers [31–37], since EDFL is a class-B laser, its dynamics is regu-

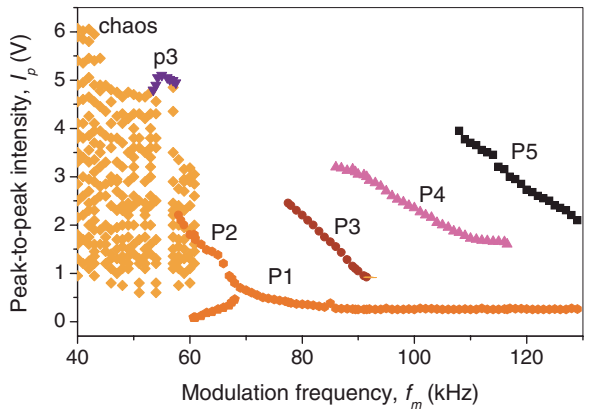

FIG. 3. (Color online) Experimental bifurcation diagram of EDFL peak-to-peak intensity with modulation frequency as a control parameter. Different attractors are shown by different colors.

lated by the main laser resonance, which appears in the vicinity of f_r. The period-3 (P3), period-4 (P4), and period-5 (P5) attractors are born and dead in the saddle-node bifurcations. The crisis and inverse period-doubling bifurcations are also seen near $f_m \approx 60$ kHz and 68 kHz, respectively, in the same manner that the P3 window within the chaotic region (chaos) is found close to $f_m = 55$ kHz. In general, a laser system modulated above its relaxation oscillation frequency is not so sensitive to pump modulation as when it is modulated below f_r. Such behavior concerns not only laser systems but also other nonlinear oscillators.

In this work, we address the following question. How does the laser system amplify intrinsic and additional external noise while approaching the critical points? In order to approach the problem, we measure the EDFL noise level in the laser power spectrum. Examples of the power spectra in the P3 regime for two different modulation frequencies are shown in Fig. 4. Spectral noise density N_m at f_m is found by connecting the average noise levels below and above the modulation frequency. One can see that the noise (ground) level for $f_m = 78$ kHz is higher than that for $f_m = 83$ kHz, i.e., $N_{m2} > N_{m1}$. This fact indicates that the laser amplifies the

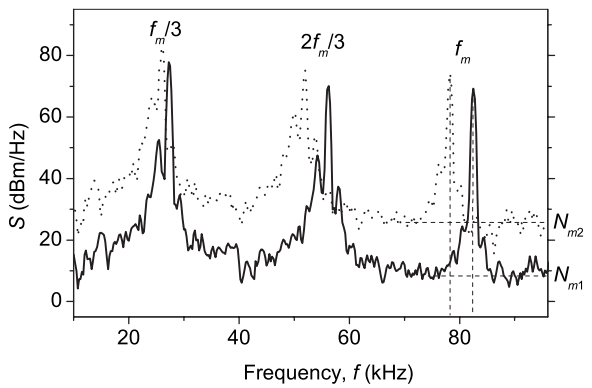

FIG. 4. Experimental EDFL power spectra for P3 regime at external noise $n = 100$ mV (~10%) for $f_m = 83$ kHz (solid line) and 78 kHz (dotted line). The horizontal dashed lines show the noise levels N_{m1} and N_{m2} at the modulation frequencies shown by the vertical dashed lines.

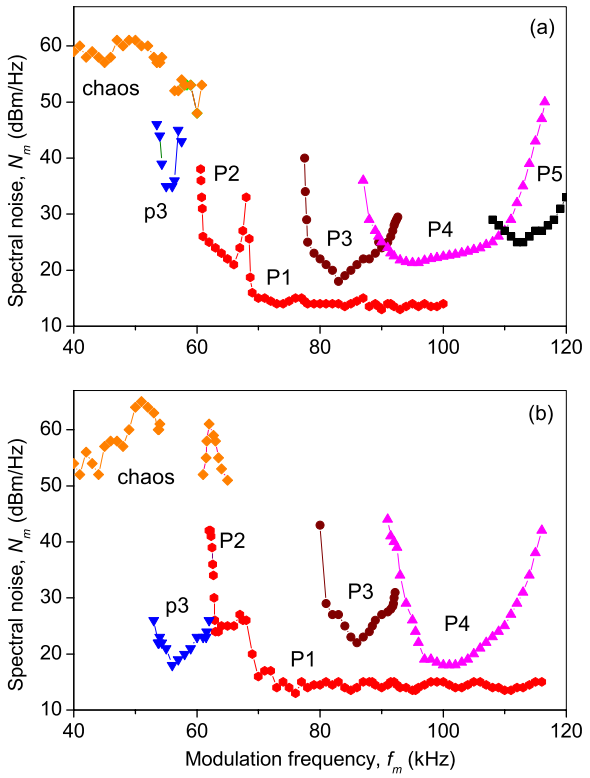

FIG. 5. (Color online) Bifurcation diagrams of spectral noise component versus modulation frequency demonstrating noise amplification near critical points for (a) intrinsic laser noise and (b) $n = 200$ mV. Various dynamical regimes are shown with different colors.

noise once f_m approaches the saddle-node bifurcation which occurs close to 78 kHz (see Fig. 3). A similar behavior is observed in the vicinity of other bifurcation points. Figure 5 shows N_m at the modulation frequency as a function of f_m for intrinsic laser noise [Fig. 5(a)] and for additive noise $n = 200$ mV (~20%) [Fig. 5(b)]. In both cases, the prebifurcation noise amplification is evident near every critical point (saddle node, period doubling, and crisis). The closer the system to the bifurcation point, the stronger the amplification becomes. The effect is more pronounced at the corresponding subharmonic frequencies for each attractor, i.e., at $f_m/3$ for P3, at $f_m/4$ for P4, and at $f_m/5$ for P5. As the period-doubling bifurcation is approached, the amplification is greater for smaller noise, in good agreement with the previously observed small-signal amplification [20,21]. As seen from Fig. 5, the noise amplification near the saddle node and crisis bifurcations can reach 30 dB, i.e., the noise amplitude is increased by three orders of magnitude while approaching these critical points. We have not found a significant difference in the character of noise amplification near different types of bifurcation. Near the saddle-node and crisis points, noise increases exponentially until the attractor disappears; whereas near the period-doubling bifurcation there is a maximum in the noise amplitude.

We should note that in our experiments, the diode pump-laser noise level and its modulation amplitude were independent of the modulation frequency because we dealt with the frequencies (<100 kHz) much lower than the relaxation os-

cillation frequency of the semiconductor laser (>1 GHz). Moreover, in the experiments on the noise amplification, the pump power was fixed and the control parameter was the modulation frequency. Thus, the noise amplification effect observed was due to only nonlinear processes in the EDFL itself but not in the pump laser.

III. THEORY

A. Model

A diode-pumped EDFL belongs to class-B lasers [39] along with solid-state, semiconductor, and CO_2 lasers. In this type of lasers, the polarization relaxation is very fast and therefore can be adiabatically eliminated, allowing the dynamics to be described by only two rate equations: one for the laser field and the second for the population inversion. The main ideas underlying the model equations for EDFL have been developed in some of our previous work (see, for instance, [34,35,37]). In the absence of external pump modulation and noise, EDFL dynamics is ruled mainly by the following processes: (i) the resonant ground-state absorption (GSA) saturation, (ii) the excited-state absorption (ESA) loss [40] and cooperative (Auger) up conversion [41,42] (both determined by the Er^{3+} ion energy levels' structure), and (iii) the amplified spontaneous emission (ASE)—an essential feature of a fiber laser with a relatively long cavity. The periodic and stochastic pump modulations are introduced into the model as "external" disturbance factors which considerably affect upon the EDFL dynamics [38].

The balance equations for EDFL generation intracavity power P_g (in s^{-1}) and dimensionless population y of the upper laser level of Er^{3+} ($^4I_{13/2}$) are written as follows:

$$\frac{dP_g}{dt} = \frac{2L_0}{T_r}[P_g\{\Gamma\alpha_0[(\xi-\eta)y-1]-\alpha_l\} + 2\Gamma\alpha_0(\xi-1)y\mu\Delta\nu_{\mathrm{Er}}K(y)\exp(-L\gamma)], \tag{1}$$

$$\frac{dy}{dt} = -\frac{\Gamma\alpha_0}{N_0S_a}P_g(\xi y-1) - \frac{y}{\tau_0}\left\{1+4[K^*(y)-1]\frac{\Gamma\alpha_0^*(\xi-1)\tau_0\Delta\nu_{\mathrm{Er}}}{N_0S_a}\right\} - \frac{y^2}{\tau_1} + \frac{1-\exp[-\delta\alpha_0L_0(1-y)]}{S_pN_0L_0h\nu_p}P_p[1+A\sin(2\pi f_mt)+n\zeta], \tag{2}$$

where $\alpha_0=N_0\sigma_{\mathrm{GSA}}$ and $\alpha_0^*\approx 2\alpha_0$ are the small-signal absorption coefficients of the active erbium-doped fiber core at the generation wavelength $\lambda_g=1.56$ μm and near the Er^{3+} emission band maximum ($\lambda^*\approx 1.53$ μm), N_0 is the Er^{3+} concentration, $\xi=1+\sigma_e/\sigma_{\mathrm{GSA}}$ and $\eta=\sigma_{\mathrm{ESA}}/\sigma_{\mathrm{GSA}}$ are the coefficients addressing the relations between the GSA, ESA, and gain cross sections at λ_g (σ_{GSA} and σ_e being the cross sections of the GSA and gain transitions between the $^4I_{15/2}$ and $^4I_{13/2}$ states and σ_{ESA} is the effective ESA cross section in Er^{3+}). τ_0 is the lifetime of single Er^{3+} ions in the excited $^4I_{13/2}$ state; τ_1 is the effective relaxation time of the Er^{3+}-Er^{3+} pair clusters, where each Er^{3+} ion forming a pair is in the excited state; $\Gamma=1-\exp(-S_a/S_w)$ is the quantity accountable for the generation wave/fiber core overlap factor ($S_a=\pi a^2$ and $S_w=\pi w_0^2/2$ being, respectively, the geometrical cross sections of the erbium-doped fiber core and the wave-guided beam, where a and w_0 are the core and beam radii); $T=2n_0L/c$ is the photon intracavity round-trip time, where L is the total cavity length being the sum of the active fiber length L_0 and the total length l_0 of all other intracavity fiber components, $n_0=1.46$ is the refractive index of silica, and c is the velocity of light in vacuum; $\alpha_l=\gamma-\ln(R_1R_2)/2L$ is the intracavity overall losses, where γ stands for the total nonresonant intracavity loss, and R_1 and R_2 are the reflection coefficients of the FBG couplers forming the EDFL cavity; $\Delta\nu_{\mathrm{Er}}$ is the Er^{3+} emission bandwidth (assumed to be homogeneously broadened); δ is the dimensionless coefficient accounting for the ratio of absorption coefficient of erbium-doped fiber at the pump wavelength λ_p to that (α_0) at the generation wavelength λ_g; $\mu=\Delta\nu_g/\Delta\nu_{\mathrm{Er}}$ is the factor addressing the ratio of the generation and spontaneous emission bandwidths; $h\nu_p$ is the pump energy quanta;S_p is the pump radiation geometrical cross section (it is assumed further that the pump radiation is effectively absorbed within the active fiber core: $S_p=\pi w_p^2\approx S_a$) and P_p (in W) is the pump power at the active fiber entrance.

The parameters responsible for the periodic and stochastic external modulation are defined as follows. A and f_m are the amplitude and frequency of sinusoidal modulation, n is the noise amplitude, and ζ is a random number ($A,n,\zeta\in[0,1]$). The quantities K and K^* are the length-averaged ASE coefficients defined as

$$K=\frac{\exp\{L_0\Gamma\alpha_0[(\xi-\eta)y-1]\}-1}{L_0\Gamma\alpha_0[(\xi-\eta)y-1]}, \tag{3}$$

$$K^*=\frac{\exp\{L_0\Gamma^*\alpha_0^*[(\xi^*-\eta^*)y-1]\}-1}{L_0\Gamma^*\alpha_0^*[(\xi^*-\eta^*)y-1]}. \tag{4}$$

In Eqs. (3) and (4), the asterisks mean that a value is taken at λ^* (for simplicity, we assume $\xi^*=\xi$, $\eta^*=\eta$, and $\Gamma^*=\Gamma$). The term $2\Gamma\alpha_0(\xi-1)y\mu\Delta\nu_{\mathrm{Er}}K(y)\exp(-L\gamma)$ in Eq. (1) characterizes the role of ASE in establishing (seeding) emission in the laser cavity, and the term $4[K^*(y)-1][\Gamma\alpha_0^*(\xi-1)\tau_0\Delta\nu_{\mathrm{Er}}]/(N_0S_a)$ in Eq. (2) expresses its influence on how the laser upper-level depopulation rate grows. The parameter values either measured experimentally or provided by the erbium fiber manufacturers are presented in Table I.

B. Numerical results

In order to check the validity of our model and ensure that the chosen parameters (Table I) correspond to the real experimental arrangement, we calculate the dependences of relaxation oscillation frequency f_r on pump power P_p without external modulation ($A=0$) for four different cases (with and without taking into account ASE and in the presence or absence of pump noise) and compare these results with the experimental ones (Fig. 2). This comparison allows one to reveal the importance of the ASE contribution upon the

TABLE I. Parameters used in numerical simulations.

λ_g	λ_p	$h\nu_p$	α_0	N_0	δ	σ_{GSA}	ξ	η
1560 nm	977 nm	2.037×10^{-19} J	0.06 cm^{-1}	2.4×10^{19} cm^{-3}	0.7	2.48×10^{-21} cm^{-2}	2.25	0.24

τ_0	τ_I	$\Delta\nu_{Er}$	μ	w_0	a	Γ	γ	L_0	l_0	R_1	R_2
100 ms	0.71 ms	25 nm	10^{-3}	2.61 μm	1.35 μm	0.417	8.7×10^{-4} cm^{-1}	0.82 m	3.51 m	1	0.91

EDFL characteristics. If ASE is considered when modeling (see curves 1 and 1′), we get a good agreement between numerically calculated and experimentally measured relaxation oscillation frequency (f_r=30 kHz) for the same excess of the pump power over the laser threshold ($\varepsilon\approx1.3$). Notice that the theoretical value obtained for the EDFL threshold (~14 mW) is very close to its experimental value (13.8 mW). Meanwhile, when ASE is ignored in modeling (see curves 2 and 2′), the model becomes very unsatisfactory. It is also remarkable that the theoretical dependences $f_r(P_p)$ obtained for a zero noise (n=0) and large noise (n=0.5) almost repeat the experimentally measured ones (compare the theoretical curves 1 and 1′ with the experimental ones). Our theory also predicts an increase of f_r when noise is added, as the experiments reveal. All the above results prove the model validity and therefore ensure its applicability to modeling EDFL dynamics at external pump modulation and noise biased.

Next, we present the temporal and spectral analyses of the time series of intracavity laser power $P_g(t)$ calculated using Eqs. (1) and (2) for various amplitudes A and frequencies f_m of pump modulation and various noise levels n at a fixed pump power level (i.e., fixed EDFL threshold). Figure 6 shows the theoretical power spectra for two different modulation frequencies, f_m=83 and 78 kHz at fixed $\varepsilon\approx1.3$ ($P_p\approx18$ mW), modulation depth (0.25), and input noise amplitude (0.25), when the laser oscillates in the period-3 regime. One can see that the noise levels (output noise) at f_m and its third subharmonic $f_m/3$ are higher for f_m=78 kHz than for f_m=83 kHz, i.e., the laser amplifies noise while approaching the saddle-node bifurcation—the birth point for the P3 attractor—as it is exactly the case in experiments (compare with Fig. 4). In this paper, we are not showing the numerically calculated bifurcation diagram of the pump-modulated EDFL intensity as a function of f_m because it is very similar to those previously published [32–34,37]; but we prove an almost exact coincidence with the experimental bifurcation diagram in Fig. 3.

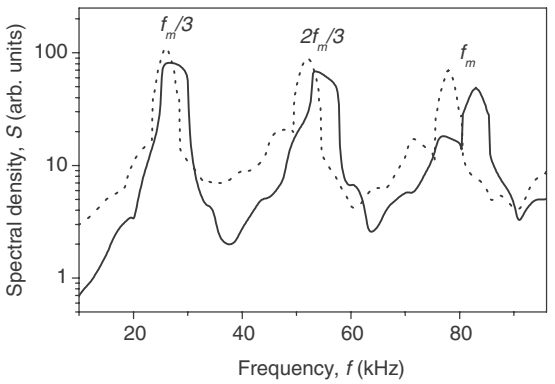

FIG. 6. Numerically calculated power spectra for modulation frequencies f_m=83 kHz (solid line) and 78 kHz (dotted line) of EDFL working in P3 regime in the presence of external noise. A=0.25 and n=0.25.

Figure 7 shows the theoretical spectral noise density N_m at the modulation frequency f_m as a function of f_m for the coexisting attractors P1, P3, and P4. As in the experiment (see Fig. 5), we notice a significant noise amplification as the laser is approaching the saddle-node bifurcation points. One can observe a good agreement between the theoretical "noise bifurcation diagram" (Fig. 7) and the measured one (Fig. 5). So, the developed EDFL model allows us to explain the increment of "noisy" background of EDFL with external modulation at approaching every bifurcation point (either saddle node or period doubling) observed in the above experiments.

IV. CONCLUSIONS

In this paper, we provided the experimental evidence of prebifurcation noise amplification near different types of bifurcations in a diode-pumped EDFL. We found that noise fluctuations were amplified not only in the vicinity of a period-doubling bifurcation as was already shown in some theoretical papers but also near saddle-node and crisis points. We revealed that the closer to the bifurcation point the system is, the stronger the noise amplification becomes. The

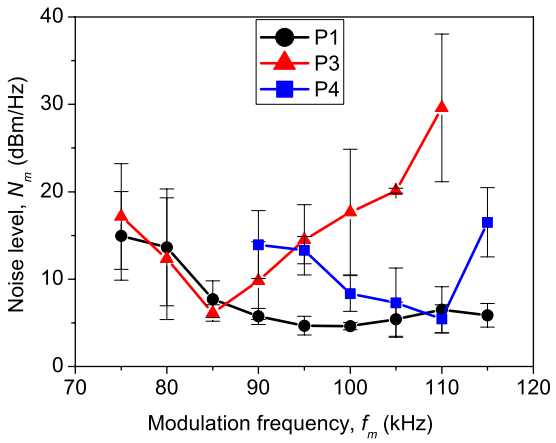

FIG. 7. (Color online) Calculated noise amplification for P1, P3, and P4 regimes as a function of modulation frequency for the same parameters as in Fig. 5.

noise amplitude increased by three orders of magnitude, while the system was approaching the saddle-node and crisis points. Near the period-doubling bifurcation, the effect was more pronounced for smaller-amplitude noise. The results of numerical simulations using the developed EDFL model demonstrated a fine agreement with the experiment. A comparison of the numerical and experimental results indicated the importance of the ASE contribution in the EDFL dynamics.

Many theoretical works have predicted generality of prebifurcation noise amplification. Our studies demonstrated with EDFL that this phenomenon can be expected near different critical points, and thus the results may have important applications for prediction of crises and catastrophes in other dynamical systems, e.g., in meteorology, geophysics, medicine, stock market, etc.

ACKNOWLEDGMENTS

This work was supported by the Mexican Council of Science and Technology (CONACYT) under Projects No. 46973 and No. 47029. A.N.P. thanks E. D. Surovyatkina for useful discussions.

[1] S. A. Akhmanov, Y. E. D'yakov, and A. S. Chirkin, *Introduction to Radiophysics and Optics* (Nauka, Moscow, 1981).
[2] A. V. Fedorov, S. L. Harper, S. G. Philander, B. Winter, and A. Wittenberg, Bull. Am. Meteorol. Soc. **84**, 911 (2003).
[3] D. Chen, M. A. Cane, A. Kaplan, S. E. Zabiak, and D. Huang, Nature (London) **428**, 733 (2004).
[4] J. V. Greenman and T. G. Benton, Am. Nat. **161**, 225 (2003).
[5] E. Surovyatkina, Nonlinear Processes Geophys. **12**, 25 (2005).
[6] D. Alonso, A. J. McKane, and M. Pascual, J. R. Soc., Interface **4**, 575 (2007).
[7] J. García-Ojalvo and R. Roy, Phys. Lett. A **224**, 51 (1996).
[8] G. Giacomelli, F. Marin, and I. Rabbiosi, Phys. Rev. Lett. **82**, 675 (1999).
[9] G. Giacomelli, M. Giudici, S. Balle, and J. R. Tredicce, Phys. Rev. Lett. **84**, 3298 (2000).
[10] V. N. Chizhevsky, E. Smeu, and G. Giacomelli, Phys. Rev. Lett. **91**, 220602 (2003).
[11] K. Kaneko, Phys. Rev. Lett. **78**, 2736 (1997); Physica E (Amsterdam) **124D**, 322 (1998).
[12] S. Kraut, U. Feudel, and C. Grebogi, Phys. Rev. E **59**, 5253 (1999).
[13] A. N. Pisarchik, *Some Topics of Modern Optics (*Rinton, Paramus, 2008), pp. 326–391.
[14] B. K. Goswami and A. N. Pisarchik, Int. J. Bifurcation Chaos Appl. Sci. Eng. **18**, 1645 (2008).
[15] C. Masoller, Phys. Rev. Lett. **88**, 034102 (2002).
[16] G. Huerta-Cuellar, A. N. Pisarchik, and Y. O. Barmenkov, Phys. Rev. E **78**, 035202(R) (2008).
[17] S. Kim, S. H. Park, and C. S. Ryu, Phys. Rev. Lett. **78**, 1616 (1997).
[18] U. Feudel, Int. J. Bifurcation Chaos Appl. Sci. Eng. **18**, 1607 (2008).
[19] K. Wiesenfeld, J. Stat. Phys. **38**, 1071 (1985).
[20] K. Wiesenfeld and B. McNamara, Phys. Rev. A **33**, 629 (1986).
[21] R. Corbalán, J. Cortit, A. N. Pisarchik, V. N. Chizhevsky, and R. Vilaseca, Phys. Rev. A **51**, 663 (1995).
[22] Y. A. Kravtsov, S. G. Bilchinskaya, O. Y. Butkovskii, I. A. Rychka, E. D. Surovyatkina, Zh. Eksp. Teor. Fiz. **120**, 1527 (2001).
[23] Y. A. Kravtsov and E. D. Surovyatkina, Phys. Lett. A **319**, 348 (2003).
[24] E. D. Surovyatkina, Phys. Lett. A **329**, 169 (2004).
[25] E. D. Surovyatkina, Y. A. Kravtsov, and J. Kurths, Phys. Rev. E **72**, 046125 (2005).
[26] C. Jeffries and K. Wiesenfeld, Phys. Rev. A **31**, 1077 (1985).
[27] O. N. Pochepen (private communication).
[28] M. F. Bocko and J. Battiato, Phys. Rev. Lett. **60**, 1763 (1988).
[29] H. Lamela, S. Perez, and G. Carpintero, Opt. Lett. **26**, 69 (2001).
[30] *Rare Earth Doped Fiber Lasers and Amplifiers*, edited by M. J. F. Digonnet (Marcel Dekker, New York, 1993).
[31] J. M. Saucedo-Solorio, A. N. Pisarchik, A. V. Kir'yanov, and V. Aboites, J. Opt. Soc. Am. B **20**, 490 (2003).
[32] A. N. Pisarchik, Y. O. Barmenkov, and A. V. Kir'yanov, IEEE J. Quantum Electron. **39**, 1567 (2003).
[33] A. N. Pisarchik, Y. O. Barmenkov, and A. V. Kir'yanov, Phys. Rev. E **68**, 066211 (2003).
[34] A. N. Pisarchik, Y. O. Barmenkov, and A. V. Kir'yanov, OSA Trends Opt. Photonics Ser. **94**, 1277 (2004).
[35] R. J. Reategui, A. V. Kir'yanov, A. N. Pisarchik, Y. O. Barmenkov, and N. N. Il'ichev, Laser Phys. **14**, 1277 (2004).
[36] A. N. Pisarchik and Y. O. Barmenkov, Opt. Commun. **254**, 128 (2005).
[37] A. N. Pisarchik, A. V. Kir'yanov, Y. O. Barmenkov, and R. Jaimes-Reátegui, J. Opt. Soc. Am. B **22**, 2107 (2005).
[38] Y. O. Barmenkov and A. V. Kir'yanov, Opt. Express **12**, 3171 (2004).
[39] *Instabilities and Chaos in Quantum Optics*, edited by F. T. Arecchi and R. G. Harrison (Springer-Verlag, New York, 1987).
[40] A. D. Guzman-Chavez, Y. O. Barmenkov, and A. V. Kir'yanov, Appl. Phys. Lett. **92**, 191111 (2008).
[41] Auger up conversion is a noticeable factor for EDF with high concentration of Er^{3+} ions in the presence of Er^{3+}-Er^{3+} pair clusters.
[42] A. V. Kir'yanov, Yu. O. Barmenkov, and N. N. Il'ichev, Opt. Express **13**, 8498 (2005).